RSC Medicinal Chemistry

ROYAL SOCIETY OF CHEMISTRY

RESEARCH ARTICLE

Cite this: *RSC Med. Chem.*, 2022, **13**, 568

Design, synthesis, and biological evaluation of new thalidomide–donepezil hybrids as neuroprotective agents targeting cholinesterases and neuroinflammation†

Cindy Juliet Cristancho Ortiz,[a] Matheus de Freitas Silva,[a] Letizia Pruccoli,[b] Nathália Fonseca Nadur,[c] Luciana Luíza de Azevedo,[c] Arthur Eugen Kümmerle,[c] Isabella Alvim Guedes,[d] Laurent Emmanuel Dardenne,[d] Luiz Felipe Leomil Coelho,[e] Marcos J. Guimarães,[f] Fernanda M. R. da Silva,[f] Newton Castro,[f] Vanessa Silva Gontijo,[a] Viviana C. T. Rojas,[g] Merelym Ketterym de Oliveira,[g] Fabiana Cardoso Vilela,[g] Alexandre Giusti-Paiva,[g] Gisele Barbosa,[h] Lídia Moreira Lima,[h] Gabriela Beserra Pinheiro,[i] Letícia Germino Veras,[i] Márcia Renata Mortari,[i] Andrea Tarozzi[ab] and Claudio Viegas Jr.*[a]

A new series of eight multifunctional thalidomide–donepezil hybrids were synthesized based on the multi-target-directed ligand strategy and evaluated as potential neuroprotective, cholinesterase inhibitors and anti-neuroinflammatory agents against neurodegenerative diseases. A molecular hybridization approach was used for structural design by combining the *N*-benzylpiperidine pharmacophore of donepezil and the isoindoline-1,3-dione fragment from the thalidomide structure. The most promising compound, PQM-189 (**3g**), showed good AChE inhibitory activity with an IC_{50} value of 3.15 μM, which was predicted by docking studies as interacting with the enzyme in the same orientation observed in the AChE–donepezil complex and a similar profile of interaction. Additionally, compound **3g** significantly decreased iNOS and IL-1β levels by 43% and 39%, respectively, after 24 h of incubation with lipopolysaccharide. *In vivo* data confirmed the ability of **3g** to prevent locomotor impairment and changes in feeding behavior elicited by lipopolysaccharide. Moreover, the PAMPA assay evidenced adequate blood–brain barrier and gastrointestinal tract permeabilities with an Fa value of 69.8%. Altogether, these biological data suggest that compound **3g** can treat the inflammatory process and oxidative stress resulting from the overexpression of iNOS and therefore the increase in reactive nitrogen species, and regulate the release of pro-inflammatory cytokines such as IL-1β. In this regard, compound PQM-189 (**3g**) was revealed to be a promising neuroprotective and anti-neuroinflammatory agent with an innovative thalidomide–donepezil-based hybrid molecular architecture.

Received 22nd November 2021,
Accepted 15th March 2022

DOI: 10.1039/d1md00374g

rsc.li/medchem

Introduction

Neuroinflammation has been implicated as a pathological hallmark in several neurodegenerative diseases (NDs), including Alzheimer's disease (AD),[1] Parkinson's disease (PD),[2] Huntington's disease (HD)[3] and multiple sclerosis.[4] NDs are characterized by protein misfolding and accumulation of some specific protein aggregates inside the cell (tau or α-synuclein) or outside the cell (β-amyloid peptide (βA)), affecting different types of neurons and causing a set of

[a] *PeQuiM-Laboratory of Research in Medicinal Chemistry, Federal University of Alfenas, 2600 Jovino Fernandes Sales Ave., Alfenas, MG 37130-840, Brazil. E-mail: cvjviegas@gmail.com*
[b] *Department for Life Quality Studies, University of Bologna'Alma Mater Studiorum', 237 Corso d'Augusto St., 47921 Rimini, Italy. E-mail: andrea.tarozzi@unibo.it*
[c] *Laboratory of Molecular Pharmacology, Institute of Biomedical Sciences, Federal University of Rio de Janeiro, 21941-902, Seropédica, RJ, Brazil*
[d] *National Laboratory for Scientific Computing, 25651-075, Petrópolis, RJ, Brazil*
[e] *Institute of Biomedical Sciences, Federal University of Alfenas, 700 Gabriel Monteiro da Silva St, Alfenas, MG 37130-840, Brazil*
[f] *Laboratory of Molecular Pharmacology, Institute of Biomedical Sciences, Federal University of Rio de Janeiro, 21941-902, Rio de Janeiro/RJ, Brazil*
[g] *Laboratory of Physiology, Federal University of Alfenas, 2600 Jovino Fernandes Sales Avenue, Alfenas, MG 37130-840, Brazil*
[h] *LASSBio - Laboratório de Avaliação e Síntese de Substâncias Bioativas, Health Sciences Center, Federal University of Rio de Janeiro, 21941-902, Rio de Janeiro/RJ, Brazil*
[i] *Laboratory of Neuropharmacology, Institute of Biological Sciences, University of Brasília, Brasilia, DF 70910-900, Brazil*

† Electronic supplementary information (ESI) available. See DOI: 10.1039/d1md00374g

signal processing impairment.[5] Under pathological conditions, toxic fragment protein deposits are accumulated in the brain and, in turn, activate immune cells, microglia and astrocytes through the release of pro-inflammatory mediators and toxins that further activate these cells, causing positive feedback as well as neuronal and glial cell damage.[4] The disproportionate release of cytokines as well as reactive oxygen and nitrogen species (ROS and RNS) causes damage of healthy neurons, synaptic dysfunction, synapse loss, and neuronal death.[6] Therefore, an imbalance between pro-inflammatory and reparative functions of neuroimmune cells may result in a neuroinflammatory condition at the central nervous system (CNS) level.[7]

It is not yet clear which is the triggering factor in NDs; however, we know that ROS and RNS are likely to promote the disease progression through interaction with the mitochondria and therefore increase oxidative damage.[8] As a consequence, the abnormal increase of these species alters neuronal functions and activates inflammatory processes that lead to neurodegeneration.[9] Protection against external agents may occur through nitric oxide (NO) generation after bacterial infection or other deleterious stimulation. In this process, inducible NO synthase (iNOS) generates NO by activating the immune response through the macrophage defense mechanism. However, overexpression of iNOS increases NO levels, causing tissue damage, and high levels of NO are implicated in the pathophysiology of complex multifactorial diseases such as PD and AD. Data from the literature indicate that selective inhibition of iNOS is an effective approach in the therapy of complex diseases by preventing the generation of RNS and treating inflammatory processes.[10,11] Additionally, interleukin-1β (IL-1β), a pro-inflammatory cytokine, increases iNOS activity and stimulates NO production.[12,13]

Recent studies have disclosed the occurence of cross-communication between cholinergic signaling and brain immune cells in several neuroinflammatory diseases.[14] In particular, one of the possible mechanisms for controlling neuroinflammation is through the activation of the "cholinergic anti-inflammatory pathway" mediated by acetylcholine (ACh) binding to α7 nicotinic acetylcholinesterase receptor (α7nAChR). According to these findings, acetylcholinesterase inhibitors (AChEIs) modulate innate immunity, probably by increasing the bioavailability of ACh in the synaptic cleft and activating the cholinergic anti-inflammatory pathway. As a result, AChEIs possess neuroprotective properties mediated by α7nAChR, and this pathway represents a new option in pharmacological intervention in neurological disorders characterized by neuroinflammation.[15] Although the current clinically approved drugs act in the decrease and momentarily slow down the symptoms of complex NDs, they are not capable of interrupting or restoring brain damage and disease progression. In the past years, considering the complex interconnection of multiple pathological factors related to the installation and progression of NDs, the design of multi-target-directed ligands (MTDLs) has emerged as a hopeful strategy for the discovery of new disease-modifying drugs. In general, this strategy is based on the molecular hybridization of different pharmacophore subunits from known biologically active chemical entities, leading to novel molecular architectures that could simultaneously modulate multiple biological targets. The combination of multiple pharmacophores into a single molecule is a challenge; nevertheless, it is expected that a single multi-target drug can bring benefits such as decreased metabolite formation and drug–drug interactions, with fewer adverse side effects and an easier therapy management by needing fewer medications to effectively treat different disease symptoms.[16]

In terms of bioactivity, the isoindole fragment and its derivatives constitute an important class of biologically active heterocyclic compounds with a diversified pharmacological profile. This fragment is present in thalidomide (**2**), initially approved as a sedative for treating morning sickness in pregnant women, but it was banned in 1961 due to reports of teratogenicity. Thalidomide is currently successfully used to treat different chronic diseases, including leprosy, multiple myeloma, cancer, Crohn's disease and AIDS, but with severe restrictions and under FDA supervision.[17] However, thalidomide has also been shown to have therapeutic effects on NDs[18,19] due to its ability to modulate several pro-inflammatory cytokines[20] and also to promote anti-apoptotic and antioxidant effects.[21]

Taking into account the anti-inflammatory effects of thalidomide (**2**), especially related to modulation of TNF-α, and the AChE inhibitory properties of donepezil (**1**), and based on the MTDL strategy, we designed a new series of potentially active multifunctional ligands (**3a**–**h**) by combining the *N*-benzylpiperazine subunit as a bioisosteric fragment of the *N*-benzylpiperidine pharmacophore of donepezil and the isoindoline-1,3-dione fragment from the thalidomide structure in a single scaffold (Fig. 1). Moreover, the isoindoline-1,3-dione moiety, a pharmacophore with anti-inflammatory properties,[22,23] was proposed to mimic the 2,3-dihydro-1*H*-indenone subunit present in donepezil and constitute a bioisosteric and second possible recognition subunit for cholinesterase inhibition. Herein, we describe the synthesis of this novel series of thalidomide–donepezil hybrids (**3a**–**h**) and the study of their anti-neuroinflammatory and anti-cholinesterase potential as neuroprotective drug candidates. We report the pharmacological evaluation of these compounds including the inhibition of cholinesterase activity, antioxidant properties and *in vitro*/*in vivo* anti-neuroinflammatory potential. In both *in vitro* and *in vivo* studies, we evaluated the ability of the target compounds to inhibit the inflammation induced by lipopolysaccharide (LPS), a component of the cell wall of Gram-negative bacteria, which has been widely used to evoke the immune system in a rodent model, triggering an inflammatory process and mimicking an infection response. After being recognized by the immune system, LPS activates an inflammatory cascade, releasing cytokines, which, upon reaching the CNS, will activate COX-2 and induce the synthesis of prostaglandins. In

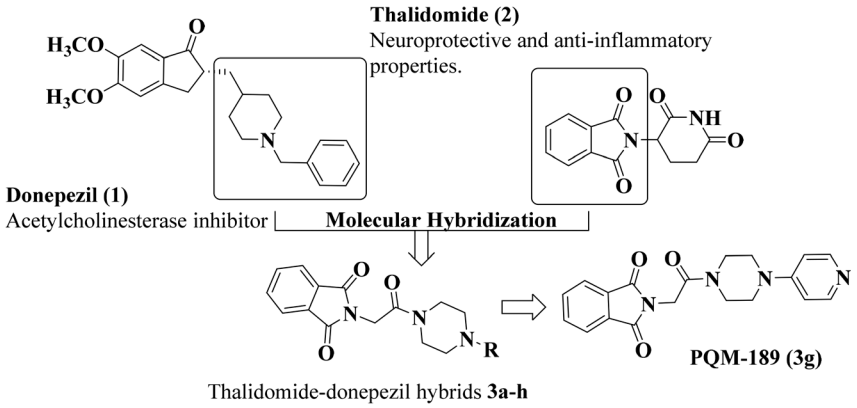

Fig. 1 Design of a new series of multifunctional thalidomide–donepezil hybrids (**3a–h**).

addition, it is possible to observe the activation of microglia and hypertrophy of astrocytes, establishing a picture of neuroinflammation.[24]

Results and discussion

Synthesis

The synthesis of the target compounds **3a–h** was based on the reaction of *N*-substituted piperazines **4a–h** with *N*-phthaloylglycine (**5**) in the presence of EDC, TEA and HOBt to provide the desired compounds **3a–h** in global yields of 60–70% (Fig. 2). All compounds were characterized by IR, NMR and HRMS techniques.

Biological results

***In vitro* AChE inhibition.** The inhibition of acetylcholinesterase (AChE) is the most widely used therapeutic approach in the treatment of AD and allows an increased level of ACh in the synaptic cleft. ACh is one of the main neurotransmitters responsible for the physiology and functionality of CNS and is involved in both learning and memory processes. Currently, donepezil is considered the first-choice drug for AD treatment due to its efficacy in the selective inhibition of AChE activity with no significant adverse effects, leading to significant cognitive and memory improvement. Thus, the modified Ellman's method[27] was used for screening the inhibitory profile of the thalidomide–donepezil hybrids (**3a–h**) against both AChE and BuChE (butyrylcholinesterase) enzymes.

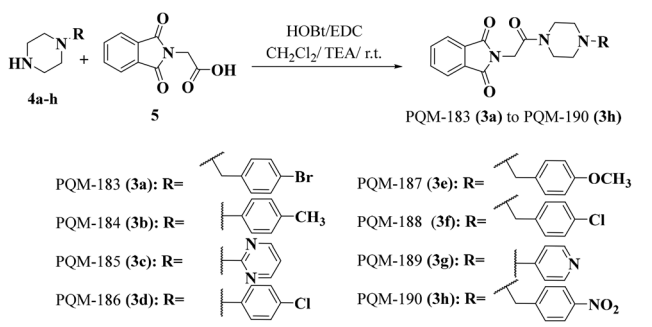

Fig. 2 Synthetic route for the preparation of the thalidomide–donepezil hybrids **3a–h**.

Preliminary results showed that only compound PQM-189 (**3g**) was capable of inhibiting 85% of AChE activity at 30 μM, with all other compounds inhibiting AChE lower than 50% at the same concentration. Additionally, at the same concentration, no compounds significantly inhibited BuChE activity (Table 1), evidencing that compound **3g** acts as a selective AChE inhibitor with an IC_{50} value of 3.15 μM. Kinetic studies (Fig. 3) revealed that **3g** was capable of binding both to the catalytic site (competitive inhibition) and to the allosteric site (non-competitive inhibition) of AChE, thereby acting in two different modes. Thus, experimental data evidenced that compound **3g** acts as a mixed-type AChE inhibitor with K_i = 0.72 μM and K'_i = 1.68 μM (Table 2).

Molecular docking study with human AChE

Considering the results from the *in vitro* AChE inhibition assay, molecular docking studies were performed with all target compounds to predict their potential binding modes at the AChE binding cavity, aiming to guide further optimization of potential hits found. Due to the significant conformational changes observed in the peripheral anionic site (PAS), three representative conformations of AChE were selected besides the structure of human AChE complexed with donepezil (PDB code 4EY7): 1ZGC (*Torpedo californica*),[28] 2CKM (*Torpedo californica*)[29] and 1Q84 (*Mus musculus*).[30] In general, all compounds of this series exhibited more favorable docking score values against the 4EY7 conformation, which was expected, since they are structurally similar to donepezil.

The three compounds predicted to have the best binding affinities were PQM-188 (**3f**, XPGscore = −16.833) > PQM-183 (**3a**, XPGscore = −16.632) > PQM-189 (**3g**, XPGscore = −13.864), interacting with the AChE binding site in the same overall orientation (Fig. 4), where the phthalimide moiety is located at the entrance of the gorge, while the phenyl group of the *N*-benzyl fragment interacts at the bottom of the cavity

Table 1 Experimental data of *in vitro* inhibition of AChE and BuChE for compounds **3a–h**

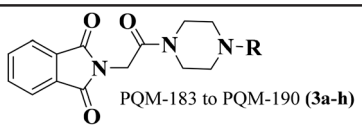

Compound	R	eeAChE % inhibition	eqBuChE % inhibition
PQM-183 (**3a**)[25]	4-Bromobenzyl	8.38	−1.37
PQM-184 (**3b**)	*p*-Tolyl	11.56	0.30
PQM-185 (**3c**)	Pyrimidin-2-yl	39.65	−5.36
PQM-186 (**3d**)[26]	4-Chlorophenyl	8.11	−2.09
PQM-187 (**3e**)	4-Methoxybenzyl	17.13	25.36
PQM-188 (**3f**)	4-Chlorobenzyl	7.82	1.26
PQM-189 (**3g**)	Pyridin-4-yl	85.0 (IC_{50} = 3.15 ± 0.63)	−4.47
PQM-190 (**3h**)	4-Nitrophenyl	16.93	−4.97

The activity is expressed as % inhibition at a concentration of 30 μM of each test compound. The concentration required for 50% inhibition (IC_{50}) of AChE was calculated only for compound **3g**, which showed the highest % inhibition at 30 μM.

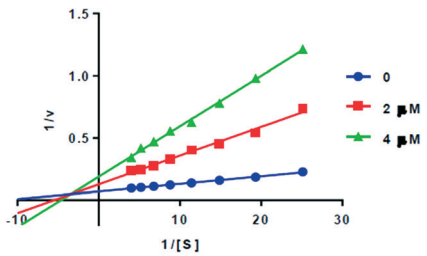

Fig. 3 Lineweaver–Burk plots for AChE inhibition by PQM-189 (**3g**).

in a similar fashion to that of donepezil. In these three highlighted compounds, the phthalimide group interacts with the Trp286 residue from the peripheral anionic site (PAS) through a π-stacking interaction and the carbonyl oxygen makes a hydrogen bond with the Phe295 main chain (NH). In PQM-183 (**3g**) and PQM-188 (**3f**), the piperazine moiety interacts through cation–π interactions with the aromatic residues Trp86, Tyr337 and Phe338 (Fig. 4A), similarly to those observed for the piperidine group from donepezil. Since PQM-183 (**3a**) and PQM-188 (**3f**) only differ in the halogen attached at the phenyl ring (*i.e.*, Br in PQM-183 (**3a**) and Cl in PQM-188 (**3f**)), they exhibit very similar binding modes and docking scores. The halogen atom of both **3a** and **3f** is located near Wat1, Ser203 and Glu202, but no halogen bonds were observed. Compound **3g** was the third compound with the best docking score (−13.864). The absence of a methylene group between the piperazine and the pyridine groups reduced the degree of flexibility of this compound and probably affected the pK_a of the nitrogen atom of the pyridine ring, which was predicted as positively charged according to Epik software. Due to this protonation state, the cationic pyridine was able to form a cation–π interaction with the Trp86 residue at the bottom of the binding cavity (Fig. 4B).

This important interaction is also observed on the AChE substrate and on a wide variety of potent AChE inhibitors.[31–33] Finally, the docking results confirmed that PQM-189 (**3g**) is a dual inhibitor against AChE, showing an experimental conformation like that observed in the AChE–donepezil complex and retaining the original orientation experimentally observed for donepezil. In addition, compound **3g** forms important interactions with Trp86, Phe295 and Trp286 residues. It is important to note that according to our initial assumptions in planning the target series, the molecular docking study evidenced the importance of the *N*-benzylpiperazine and *N*-benzylpiperidine (from donepezil) subunits, which seem to operate as bioisosteric groups, to promote the necessary interactions at the CAS site, which according to the results from the *in vitro* assays appear to be essential in the AChE inhibitory process.

ADME prediction *in silico*

In silico analysis was performed to predict the efficacy of the compounds against their molecular target and determine the ADME parameters (absorption, distribution, metabolism and excretion) that give an idea of the possible pharmacokinetics of the synthesized substances. Molecular structure is an important factor to predict the pharmacokinetic profile of

Table 2 Kinetic parameters of compound PQM-189 (**3g**) against AChE

Concentration (μM)	V_{max} ± SD[a] (μM min^{-1})	K_m ± SD[b] (μM)	K_i (μM) ± SD[c]	K'_i (μM) ± SD[d]
0	16.37 ± 0.366	125.93 ± 4.92	0.72 ± 0.007	1.68 ± 0.020
2	8.37 ± 0.428	156.00 ± 10.75		
4	7.30 ± 0.215	253.70 ± 11.9		

[a] Maximum velocity of the enzyme. [b] Michaelis constant. [c] Competitive constant. [d] Non-competitive constant; data are shown as mean ± SD of triplicate independent experiments.

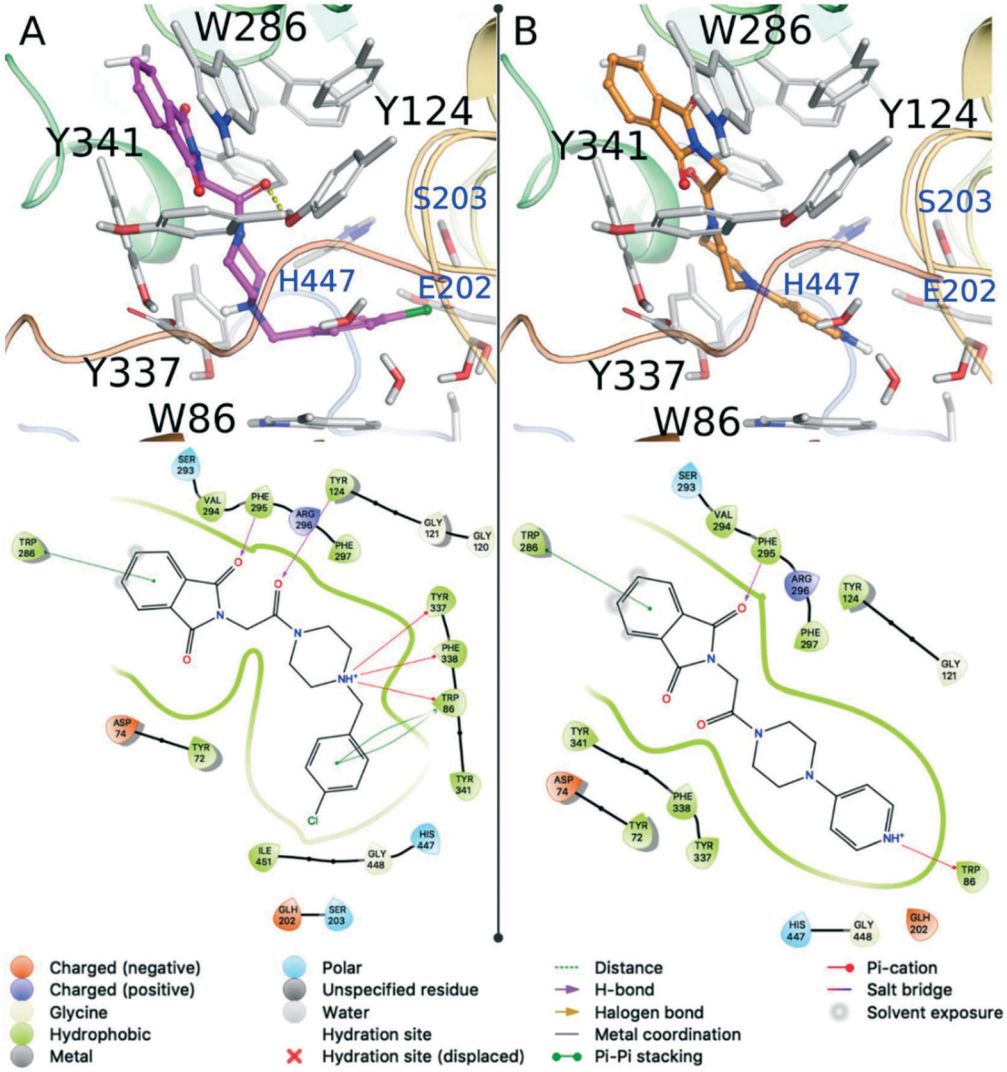

Fig. 4 Predicted binding modes for PQM-188 (**3f**) (A) and PQM-189 (**3g**) (B) against the 4EY7 conformation of AChE. Residues making hydrogen bonds or stacking interactions with the ligand are labeled black. Other important residues are highlighted in blue. Hydrogen bonds are represented as yellow dashes in the 3D picture. The ligand diagram interaction is illustrated bellow the respective 3D image.

small molecules. Based on the molecular structure, we selected some ADME properties provided from the QikProp (Schrödinger) module including lipophilicity, solubility, human oral absorption, and permeability. The QikProp module from the Schrödinger suite provides ranges for comparing a particular molecule property. The values of the observed properties are presented in Table 3.

In silico ADME data

Aqueous solubility QlogS for our compounds was predicted to range from −2.21 to −4.49. Compounds with values less than −6 are poorly soluble. Lipophilicity was evaluated using the logarithm of the *n*-octanol/water partition coefficient $QlogP_{o/w}$. Partition coefficients are useful in the estimation of drug distribution within the organism.[34] Higher lipophilicity makes it more likely to penetrate the BBB. Good permeability and solubility associated with a moderate QlogP ($0 < \log P <$ 3). For the synthesized compounds, the predicted values of partition coefficients ranged from 1.07 to 2.58. However, the percentage of oral human absorption of our series lead compound **3g** was moderate, with a value of 76%. On the other hand, the ability to cross the blood–brain barrier (BBB) is expected to be one of the positive characteristics of the compounds to reach the CNS. BBB permeability values of our compounds were predicted to range from −0.31 to −1.91, and compound **3g** is predicted to be inactive in the CNS (−2), which is indeed required for good drug candidature. Donepezil was included for comparison purposes (Table 3).

Cytotoxicity and antioxidant activity

The cytotoxicity of compounds **3a–h** was investigated in human neuronal SH-SY5Y cells to select the range of concentrations not associated with cytotoxicity. Cells were treated for 24 h with various concentrations of compounds

Table 3 *In silico* ADME data from QikProp v.3.5 software (Schrödinger) for the most active multitarget lead compounds and donepezil

Compound	Molecular volume[a]	QPlog$P_{o/w}$[b]	QPlogS[c]	QPlogHERG[d]	QPlogBB[e]	QPlogK_{hsa}[f]	QPPMDCK[g]	QPlogK_p[h]	CNS[i]	% human oral absorption[j]	Human oral absorption[k]
PQM 183	1229.953	2.12	−2.935	−5.602	−0.31	−0.443	240.718	−4.257	1	77.158	3
PQM 184	1174.164	2.41	−4.341	−4.782	−0.847	−0.253	311.285	−2.566	−1	88.877	3
PQM 185	1098.222	1.099	−2.858	−4.726	−1.036	−0.874	186.166	−2.893	−2	77.51	3
PQM 186	1158.1	2.588	−4.498	−4.783	−0.663	−0.299	767.407	−2.535	0	89.921	3
PQM 187	1253.102	1.603	−2.212	−5.572	−0.561	−0.619	90.962	−4.185	1	74.139	3
PQM 188	1220.948	2.04	−2.814	−5.573	−0.318	−0.469	223.94	−4.254	1	76.695	3
PQM 189	1101.684	1.077	−2.822	−4.66	−1.084	−0.864	160.269	−3.009	−2	76.299	3
PQM 190	1189.395	1.345	−3.818	−4.831	−1.937	−0.518	30.981	−4.275	−2	66.051	3
Donepezil	1266.695	4.368	−4.477	−6.608	0.189	0.569	485.175	−2.921		100	3
Value of reference (VR)	500.0–2000.0	−2–6.5	−6.5–0.5	<−5 (not good)	−3–1.2	−1.5–1.5	<25 poor, >500 great	−8.0–−1.0	−2–+2	<25% is low	−1.5–1.5

VR = gap or recommended value for 95% of known drugs (source: QikProp 3.2 user manual – Schrödinger software). [a] Total solvent-accessible volume in cubic angstroms using a probe with a 1.4 Å radius. [b] Predicted octanol/water partition coefficient. [c] Predicted aqueous solubility, log *S*. *S* in mol dm^{-3} is the concentration of the solute in a saturated solution that is in equilibrium with the crystalline solid. [d] Predicted IC_{50} value for blockage of HERG K^+ channels. [e] Predicted brain/blood partition coefficient. Note: QikProp predictions are for orally delivered drugs; for example, dopamine and serotonin are CNS negative because they are too polar to cross the blood–brain barrier. [f] Prediction of binding to human serum albumin. [g] Predicted apparent MDCK cell permeability in nm s^{-1}. MDCK cells are considered to be a good mimic for the blood–brain barrier. QikProp predictions are for non-active transport. [h] Predicted skin permeability, log K_p. [i] Predicted central nervous system activity on a −2 (inactive) to +2 (active) scale. [j] Predicted human oral absorption on 0 to 100% scale. [k] Predicted qualitative human oral absorption: 1, 2, or 3 for low, medium, or high.

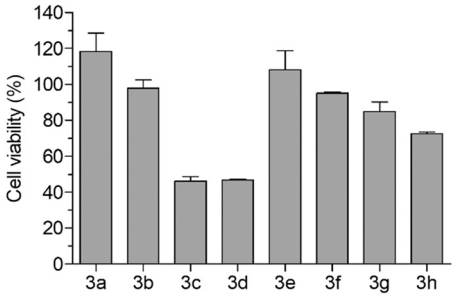

Fig. 5 Cytotoxicity of compounds **3a–h** in SH-SY5Y cells. Cells were incubated for 24 h with compounds **3a–h** at a concentration of 80 μM. At the end of incubation, cell viability was measured by MTT assay. Data are reported as mean ± SEM of three independent experiments.

3a–h (2.5–80 μM), and at the end of incubation the cell viability was measured by MTT assay. As reported in Fig. 5, compounds **3a** and **3b** and **3e–h** did not show cytotoxicity at the concentration of 80 μM, while compounds **3c** and **3d** at the same concentration showed cytotoxicity with a decrease of cell viability of 50%. The treatment of cells with all the compounds at concentrations lower than 40 μM did not affect cell viability. Therefore, we selected the range of 10–30 μM to perform the following biological assays.

The absence of cytotoxicity of the most active compound **3g** in AChE inhibition was also confirmed in the VERO cell line, a suitable model for studying the toxicity of new drug candidates.[35,36] All the compounds **3a–h** were additionally screened by potential antioxidant properties (radical scavenging capacity) in the DPPH assay at different concentrations (1.56–200 μM). Each target compound was added to a DPPH (2,2-diphenyl-1-picrylhydrazyl) solution and after a 30 min period the absorbance was recorded. However, none of the thalidomide–donepezil hybrids showed antioxidant activity, probably due to the absence of favorable structural characteristics to apply radical scavenging ability.

Parallel artificial membrane permeability assay (PAMPA)

The permeability profile through the gastrointestinal tract (GIT) and blood–brain barrier (BBB) of the target compounds was evaluated using the parallel artificial membrane permeability (PAMPA) test.[37,38] The permeability result for PAMPA-GIT classifies the compounds according to the percentage of absorbed fraction (Fa%) as high intestinal permeability (70–100%), medium permeability (30–69%) or low permeability (0–29%).[39] The PAMPA-BBB model classifies the compounds only as permeable (BBB+) or non-permeable (BBB−).[38,40]The permeability result for PAMPA-GIT classifies the compounds according to the percentage of absorbed fraction (Fa%) as high intestinal permeability (70–100%), medium permeability (30–69%) or low permeability (0–29%). The PAMPA-BBB model classifies the compounds only as permeable (CNS+) or non-permeable (CNS−).

Compound **3g** displayed high permeability through BBB, determined by the PAMPA-BBB test (Pe 13.89 × 10^{-6} cm s^{-1}), being considered CNS+ (Pe > 4.0). In addition, this compound showed moderate permeability across GIT, with Pe 3.15 × 10^{-6} cm s^{-1} and Fa 69.8%. Although *in silico* prediction showed that our lead compound **3g** was inactive in the CNS, the permeability test indicated a positive response, demonstrating that *in silico* studies must be confirmed and are only a guide to know and understand the potential of new compounds. All data are available in the ESI.†

In vitro anti-inflammatory activity and neuronal plasticity

The gene expression of iNOS and pro-inflammatory cytokines, including IL-1β and COX-2, was evaluated in microglial THP-1 cells after 24 h of treatment with LPS (1 μg mL^{-1}) in the presence of compound PQM-189 (**3g**, 10 μM) by RT-PCR. As shown in Fig. 6, compound **3g** significantly decreased iNOS and IL-1β levels with 43% and 39% of inhibition, respectively, with no significant effect on COX-2 expression.

In parallel, we evaluated the ability of **3g** to promote neuronal plasticity in terms of synaptophysin (SYP) and brain-derived neurotrophic factor (BDNF) gene expression in neuroblastoma SH-SY5Y cells after differentiation to mature neuron-like phenotype. As a result, compound **3g** significantly promoted the expression of SYP, but not BDNF, in differentiated SH-SY5Y cells (Fig. 7).

In vitro activity against Aβ-aggregates

In order to complete the investigation of PQM-189 (**3g**), its possible effect on disaggregation of $A\beta_{1-42}$ was assessed with fluorescence detection of thioflavin. In the $A\beta_{1-42}$ disaggregation test, the ThT fluorescence test was able to identify **3g** and $A\beta_{1-42}$ control (treatment: $F_{(2,19)} = 62.12$, $p < 0.0001$; time: $F_{(4,76)} = 11.74$, $p < 0.0001$ and interaction $F_{(8,76)} = 3.275$, $p = 0.0029$). Two-way ANOVA test with Bonferroni *post hoc* test showed no significant difference when compared to the test compound **3g** and $A\beta_{1-42}$ control. Moreover, regarding the endpoint, compound **3g** did not show a disaggregating effect of $A\beta_{1-42}$ comparing the H_20

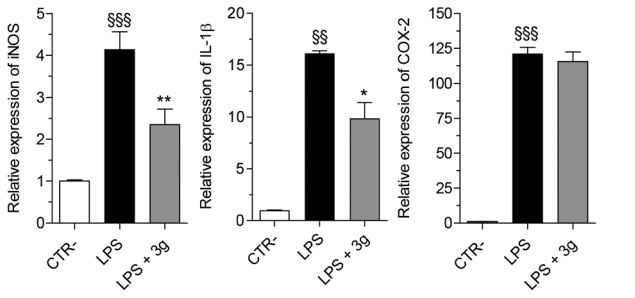

Fig. 6 *In vitro* anti-inflammatory activity of compound **3g** against LPS-induced inflammation in microglial THP-1 cells. Cells were incubated for 24 h with compound **3g** (10 μM) and LPS (1 μg mL^{-1}). At the end of incubation, iNOS, IL-1β and COX-2 expression was measured by quantitative RT-PCR. Data are reported as mean ± SEM of three independent experiments ($^{§§§}p < 0.001$ and $^{§§}p < 0.01$ *vs.* untreated cells; $^{**}p < 0.01$ and $^{*}p < 0.05$ *vs.* cells treated with LPS at one-way ANOVA with Bonferroni *post hoc* test).

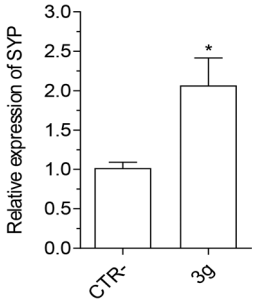

Fig. 7 Effect of compound **3g** on SYP gene expression in differentiated SH-SY5Y cells. Cells were incubated for 24 h with compound **3g** (10 μM). At the end of incubation, SYP expression was measured by quantitative RT-PCR. Data are reported as mean ± SEM of three independent experiments (*$p < 0.05$ *vs.* untreated cells with Student's *t*-test).

group, $A\beta_{1-42}$ group and the effect of PQM-189 (**3g**) ($F_{(2,19)} = 72.19$, $p < 0.0001$).

In vivo feeding and open field behavior

To evaluate the effect of compound PQM-189 (**3g**) against an inflammatory-like condition, a group of adult male Wistar rats received an intraperitoneal administration of lipopolysaccharide (LPS). As shown in Fig. 8, after a 24 h period, we observed a significant reduction in food intake in the vehicle + LPS group ($p < 0.001$) when compared to the vehicle + saline group. However, pretreatment with compound **3g** was able to prevent the reduction in feeding behavior induced by LPS; that is, there was an increase in food intake in adult male Wistar rats in the **3g** + LPS group ($p < 0.01$) when compared to the vehicle + LPS group (LPS factor: $F_{(3,96)} = 183.60$, $p < 0.001$; **3g** factor: $F_{(3,96)} = 18.04$, $p < 0.001$; LPS + **3g** factor: $F_{(9,96)} = 6.42$, $p < 0.001$). This result not only shows that compound **3g** does not negatively influence adult male rats' behavior, but quite the opposite, it was able to counteract the LPS-induced inflammatory symptoms, since loss of appetite is a common sickness behavior.

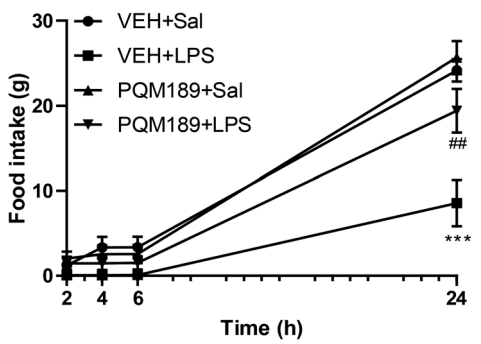

Fig. 8 Food intake 2, 4, 6 and 24 h after application of LPS in adult male Wistar rats that received pretreatment with vehicle or PQM-189 (**3g**). ***$p < 0.001$ when compared to VEH + Sal group; ##$p < 0.01$ when compared to VEH + LPS group. VEH: vehicle; Sal: saline.

Open field behavioral test

Sickness-like behavior induced by LPS was measured by locomotory activity in the open field test. LPS administration in general evaluates the autonomous behavior, curiosity, and inquiry behavior in new environments. The total distance traveled and number of standing events are used to assess locomotor activity. In this behavioral test, as depicted in Fig. 9, we observed that after 2 h of LPS administration, adult male Wistar rats showed an increase in immobility time ($p < 0.001$) when compared to the control (VEH + saline group). Meanwhile, pretreatment with PQM-189 (**3g**) significantly prevented the reduction in traveled distance and led to a decrease in immobility time induced by LPS, since there was no difference between the **3g** + LPS group when compared to the VEH + saline group (A: LPS factor: $F_{(1,23)} = 26.64$, $p < 0.001$; **3g** factor: $F_{(1,23)} = 3.54$, $p > 0.05$; LPS + **3g** factor: $F_{(1,23)} = 3.52$, $p > 0.05$; B: LPS factor: $F_{(1,23)} = 22.82$, $p < 0.001$; **3g** factor: $F_{(1,23)} = 2.07$, $p > 0.05$; LPS + **3g** factor: $F_{(1,23)} = 4.07$, $p > 0.05$).

Discussion

Nowadays, it is very well documented in the literature that neuroinflammation is a central player in the onset, progress and severity of major NDs, such as AD and PD. Moreover, a complex network of interconnected events such as protein deposition (*e.g.* Aβ and tau in AD, α-synuclein in PD), OS, and activation of microglia, astrocyte and the immune system could contribute decisively to the installation and progress of the inflammation process into the CNS.[41–46]

On the other hand, it is well described that free LPS in the bloodstream binds to lipopolysaccharide binding protein (LBP) to form the LBP–LPS complex, which activates different

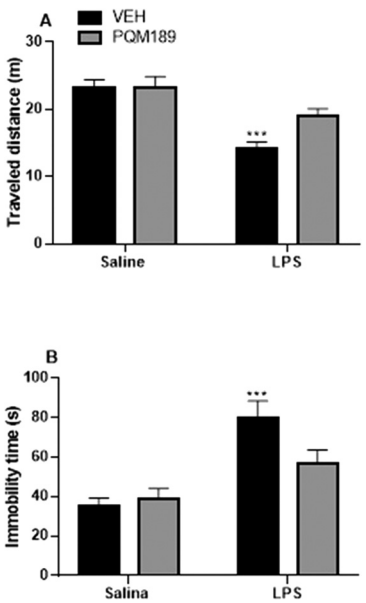

Fig. 9 Effect of pretreatment with PQM-189 (**3g**) on LPS-induced neuroinflammation in the open field test. (A) Traveled distance in meters (m) and (B) immobility time in seconds (s). ***$p < 0.001$ when compared to VEH + saline. VEH: vehicle.

inflammatory-related cell populations (monocyte, neutrophils, and macrophages) by binding to its CD14 and TLR4 receptors. Thus, one of the clearest consequences of this activation is the production of pro-inflammatory cytokines (TNF-α, IL-1 and IL-6), which act on the CNS and activate COX-2 and prostaglandin E synthase, which, in turn, stimulate the synthesis of PGE2.[47] Once the concentration of PGE2 is increased, it promotes activation of the HPA axis and neurons in the preoptic area, leading to the development of the febrile response.[48–50]

Norden *et al.*[51] reported that the activation of the immune system by LPS is also capable of inducing a coordinated response in the CNS, which could interpret and propagate inflammatory signals in the brain and, in turn, affect physiological and behavioral events. In response to these changes at the immunological and endocrine levels and in the glial face of an inflammatory-infectious stimulus, behavioral and thermoregulatory changes were observed in adult male Wistar rat models. Emphasizing the behavioral parameter, studies have shown that LPS-induced behavioral impairments including increased immobile time, low curiosity, and lack of appetite.[52,53] In this regard, more recent studies also report that the inflammation elicited by LPS can affect both the cholinergic activity and the neuronal plasticity, similarly to the observed changes in AD, suggesting an interaction among different players on behavior and neuroinflammatory response.[54–56]

Among all the tested thalidomide–donepezil hybrids, PQM-189 (**3g**) showed the most significant ability to inhibit both the AChE activity and neuroinflammation in *in vitro* models, but no significant effect was observed on disaggregation of Aβ. Interestingly, **3g** also exhibited the property to stimulate the gene expression of SYP, suggesting its ability to prevent the impairment of synaptic plasticity evoked by inflammatory and neurodegenerative processes. In this regard, PQM-189 (**3g**) may retain some of the neuroprotective effects of donepezil, as expected. In fact, recent studies have shown the contribution of donepezil to facilitating the recovery of synaptic protein impairment in different animal models.[57,58]

In addition, our *in vivo* studies confirmed the ability of PQM-189 (**3g**) to prevent the impairment of locomotor activity and feeding behavior elicited by LPS. Adult male Wistar rats that received LPS showed a reduction in the traveled distance and an increase in immobility time in the open field model. In contrast, pretreatment with **3g** was able to prevent these effects induced by endotoxin. When the feeding behavior was evaluated, a decrease in food intake was noticed 24 h after the administration of LPS. However, when adult male Wistar rats were treated with PQM-189 (**3g**) before LPS administration, the food intake was increased when compared to that of the VEH + LPS group. These findings allow us to suggest that the treatment with PQM-189 (**3g**) before the administration of LPS can prevent the behavioral changes induced by endotoxin regarding locomotor activity and feeding behavior through its ability to target the cholinergic system, in addition to neuroinflammation and synaptic dysfunction.

Finally, although the *in silico* ADME parameters results did not indicate a positive relationship for compound **3g** to cross the BBB and reach the CNS, the PAMPA permeability assays showed that compound **3g** displayed high permeability through the BBB, being considered CNS+, and showed moderate permeability across the GIT.

Experimental section

Chemistry

Infrared (IR) spectra were generated using an infrared spectrometer (Thermo Scientific USA, Nicolet iS50 model) coupled to a Pike Gladi ATR Technologies spectrometer in the Laboratory of Analysis and Characterization of Drugs (LACFar) at Federal University of Alfenas (UNIFAL-MG). ^{1}H and ^{13}C nuclear magnetic resonance (NMR) spectra were obtained on a Bruker AC-300 spectrometer operating at 300 MHz for ^{1}H NMR and 75 MHz for ^{13}C NMR. The samples were solubilized in deuterated chloroform using tetramethylsilane as the internal reference. Mass spectrometry analyses were performed in a *m*/*z* range of 80–1000 in a Bruker Compass mass spectrometer by electrospray ionization. The purity of compounds was determined by high-performance liquid chromatography (HPLC). Thin layer chromatography experiments were performed on silica gel sheet 60 F254 (Merck) and purification by chromatography column was performed on flash silica gel (220–440 mesh, 0.035–0.075 mm, Sigma-Aldrich). The visualization of the substances was done in a UV chamber (λ = 254 or 365 nm). The melting point was determined using Mars equipment (PFM II) with crushed sample and packaged in a capillary tube. All spectra are available in the ESI.†

Synthesis of thalidomide–donepezil hybrids 3a–h

Compounds **3a–h** were obtained according to the methodology of Anil K. Singh and co-workers.[59] To a solution of *N*-phthaloylglycine (2.5 mmol) in dichloromethane (15 mL), *N*-(3-dimethylaminopropyl)-*N*′-ethylcarbodiimide hydrochloride (EDC·HCl, 2.5 mmol) and triethylamine (TEA, 5.1 mmol) were added, and the reaction mixture was stirred at 0 °C for 15 min. Then, hydroxybenzotriazole (HOBT, 2.5 mmol) was added and the reaction mixture was stirred for an additional 15 min at 0 °C. After this initial period of 30 min, commercially available *N*-substituted piperazines (**5a–h**) were added and the reaction mixture was stirred for another 24 h at room temperature. Then, the solvent was removed, and the resultant crude product was extracted with ethyl acetate, washed with water, dried with anhydrous $MgSO_4$ and filtered. The organic layer was concentrated under reduced pressure to give the desired products, which were purified by flash column chromatography using dichloromethane–methanol (9.5 : 0.5) as the eluent or filtered and recrystallized from ethyl acetate or a mixture of ethyl acetate/hexane (7 : 3) to give the desired pure products **3a–h**. All compounds were

characterized by IR, ^{1}H and ^{13}C NMR and HRMS. All spectra are available in the ESI† (Fig. S1–S40).

2-(2-(4-(4-Bromobenzyl)piperazin-1-yl)-2-oxoethyl)-isoindoline-1,3-dione PQM-183 (3a). Yellow light solid (yield 32%), m.p. 156 °C. IR (ATR): *ν* 2938, 2915, 1776, 1711 and 1667 cm^{-1}. ^{1}H NMR (300 MHz, $CDCl_3$) *δ* 7.86 (dd, *J* = 3.0 and 5.6 Hz, 2H, Ar–H), 7.71 (dd, *J* = 3.0 and 5.6 Hz, 2H, Ar–H), 7.45 (d, *J* = 8.4 Hz, 2H, Ar–H), 7.21 (d, *J* = 8.4 Hz, 2H, Ar–H), 4.48 (s, 2H, CH_2CO), 3.61 (t, 2H, NCH_2CH_2N), 3.52 (t, 2H, NCH_2CH_2N), 3.48 (s, 2H, CH_2), 2.50 (t, 2H, NCH_2CH_2N), 2.43 (t, 2H, NCH_2CH_2N). ^{13}C NMR (75 MHz, $CDCl_3$) *δ* 168.1, 163.9, 136.7, 134.1, 132.3, 131.5, 130.9, 123.5, 121.2, 62.1, 52.5, 52.2, 44.8, 42.3 and 39.1. HR-MS (ESI) *m*/*z*: calcd for $C_{21}H_{20}BrN_3O_3$ $[M + H]^+$: 442.0766, found: 442.0758.

2-(2-Oxo-2-(4-(*p*-tolyl)piperazin-1-yl)ethyl)isoindoline-1,3-dione PQM-184 (3b). Yellow light solid (yield 55%), m.p. 192 °C. IR (ATR): *ν* 2989, 2908, 1778, 1706, 1638 and 1513 cm^{-1}. ^{1}H NMR (300 MHz, $CDCl_3$) *δ* 7.88 (dd, *J* = 3.0 and 5.5 Hz, 2H, Ar–H), 7.72 (dd, *J* = 3.0 and 5.5 Hz, 2H, Ar–H), 7.10 (d, *J* = 8.1 Hz, 2H, Ar–H), 6.86 (d, *J* = 8.1 Hz, 2H, Ar–H), 4.54 (s, 2H, CH_2-CO), 3.76 (t, 2H, NCH_2CH_2N), 3.69 (t, 2H, NCH_2CH_2N), 3.22 (t, 2H, NCH_2CH_2N), 3.12 (t, 2H, NCH_2CH_2N), 2.28 (s, 3H, CH_3). ^{13}C NMR (75 MHz, $CDCl_3$) *δ* 168.1, 164.0, 148.8, 134.1, 132.3, 130.4, 129.8, 123.6, 117.2, 50.1, 49.9, 44.8, 42.3, 39.1 and 20.5. HR-MS (ESI) *m*/*z*: calcd for $C_{21}H_{21}N_3O_3$ $[M + H]^+$: 364.1661, found: 364.1641.

2-(2-Oxo-2-(4-(pyrimidin-2-yl)piperazin-1-yl)ethyl)-isoindoline-1,3-dione PQM-185 (3c). White solid (yield 70%), m.p. 258 °C. IR (ATR): 2990, 2808, 1778, 1704, 1637 and 1515 cm^{-1}. ^{1}H NMR (300 MHz, $CDCl_3$) *δ* 8.33 (d, *J* = 4.7 Hz, 2H, Ar–H), 7.87 (dd, *J* = 3.1 and 5.4 Hz, 2H, Ar–H), 7.72 (dd, *J* = 3.1 and 5.4 Hz, 2H, Ar–H), 6.55 (t, 2H, Ar–H), 4.55 (s, 2H, CH_2-CO), 3.97 (t, 2H, NCH_2CH_2N), 3.86 (t, 2H, NCH_2CH_2N). 3.69 (t, 2H, NCH_2CH_2N), 3.61 (t, 2H, NCH_2CH_2N). ^{13}C NMR (75 MHz, $CDCl_3$) *δ* 168.0, 164.3, 161.5, 157.8, 134.1, 132.3, 123.6, 110.6, 44.6, 43.4, 42.1 and 39.2. HR-MS (ESI) *m*/*z*: calcd for $C_{18}H_{17}N_5O_3$ $[M + Na]^+$: 374.1229, found: 374.1209.

2-(2-(4-(4-Chlorophenyl)piperazin-1-yl)-2-oxoethyl)-isoindoline-1,3-dione PQM-186 (3d). White solid (yield 36%), m.p. 230 °C. IR (ATR): *ν* 2989, 2813, 1778, 1704 and 1639 cm^{-1}.^{1}H NMR (300 MHz, $CDCl_3$) *δ* 7.87 (dd, *J* = 3.0 and 5.5 Hz, 2H, Ar–H), 7.72 (dd, *J* = 3.0 and 5.5 Hz, 2H, Ar–H), 7.23 (d, *J* = 9.1 Hz, 2H, Ar–H), 6.85 (d, *J* = 9.1 Hz, 2H, Ar–H), 4.53 (s, 2H, CH_2CO), 3.75 (t, 2H, NCH_2CH_2N), 3.69 (t, 2H, NCH_2CH_2N), 3.24 (t, 2H, NCH_2CH_2N), 3.14 (t, 2H, NCH_2CH_2N). ^{13}C NMR (75 MHz, $CDCl_3$) *δ* 168.0, 164.0, 149.4, 134.1, 132.3, 129.2, 125.7, 123.6, 118.0, 49.5, 49.3, 44.6, 42.1 and 39.1. HR-MS (ESI) *m*/*z*: calcd for $C_{20}H_{18}ClN_3O_3$ $[M + Na]^+$: 406.0934, found: 406.0915.

2-(2-(4-(4-Methoxybenzyl)piperazin-1-yl)-2-oxoethyl)-isoindoline-1,3-dione PQM-187 (3e). White solid (yield 41%), m.p. 166 °C. IR (ATR): *ν* 2928, 2831, 1772, 1709, 1656 and 1513 cm^{-1}. ^{1}H NMR (300 MHz, $CDCl_3$) *δ* 7.86 (dd, *J* = 3.1 and 5.4 Hz, 2H, Ar–H), 7.71 (dd, *J* = 3.1 and 5.4 Hz, 2H, Ar–H), 7.23 (d, *J* = 8.7 Hz, 2H, Ar–H), 6.86 (d, *J* = 8.7 Hz, 2H, Ar–H), 4.47 (s, 2H, CH_2CO), 3.80 (s, 3H, OCH_3), 3.60 (t, 2H, NCH_2CH_2N), 3.52 (t, 2H, NCH_2CH_2N), 3.48 (s, 2H, CH_2), 2.50 (s, 2H, CH_2), 2.43 (t, 2H, NCH_2CH_2N). ^{13}C NMR (75 MHz, $CDCl_3$) *δ* 168.1, 163.8, 158.9, 134.0, 132.3, 130.3, 129.5, 123.5, 113.7, 62.2, 55.3, 52.6, 52.4, 44.8, 42.3 and 39.1. HR-MS (ESI) *m*/*z*: calcd for $C_{22}H_{23}N_3O_4$ $[M + H]^+$: 394.1759, found: 394.1759.

2-(2-(4-(4-Chlorobenzyl)piperazin-1-yl)-2-oxoethyl)-isoindoline-1,3-dione PQM-188 (3f). White solid (yield 27%), m.p. 146 °C. IR (ATR): *ν* 2940, 2816, 1776, 1712 and 1688 cm^{-1}. ^{1}H NMR (300 MHz, $CDCl_3$) *δ* 7.86 (dd, *J* = 3.0 and 5.4 Hz, 2H, Ar–H), 7.71 (dd, *J* = 3.0 and 5.4 Hz, 2H, Ar–H), 7.36–7.12 (m, 4H, Ar–H), 4.47 (s, 2H, CH_2CO), 3.60 (t, 2H, NCH_2CH_2N), 3.52 (t, 2H, NCH_2CH_2N), 3.50 (s, 2H, CH_2), 2.50 (t, 2H, NCH_2CH_2N), 2.43 (t, 2H, NCH_2CH_2N). ^{13}C NMR (75 MHz, $CDCl_3$) *δ* 168.1, 163.9, 136.2, 134.1, 133.1, 132.3, 130.3, 128.5, 123.5, 62.0, 52.7, 52.5, 44.8, 42.3 and 39.1. HR-MS (ESI) *m*/*z*: calcd for $C_{21}H_{20}ClN_3O_3$ $[M + H]^+$: 398.1271, found: 398.1271.

2-(2-Oxo-2-(4-(pyridin-4-yl)piperazin-1-yl)ethyl)isoindoline-1,3-dione PQM-189 (3g). White solid (yield 32%), m.p. 238 °C. IR (ATR): *ν* 2897, 2857, 1769, 1716, 1651 and 1512 cm^{-1}. ^{1}H NMR (300 MHz, $CDCl_3$) *δ* 8.31 (d, *J* = 5.6 Hz, 2H, Ar–H), 7.87 (dd, *J* = 3.0 and 5.2 Hz, 2H, Ar–H), 7.72 (dd, *J* = 3.0 and 5.2 Hz, 2H, Ar–H), 6.66 (d, *J* = 5.6 Hz, 2H, Ar–H), 4.53 (s, 2H, CH_2-CO), 3.82–3.62 (m, 4H, NCH_2CH_2N), 3.49 (t, 2H, NCH_2CH_2N), 3.39 (t, 2H, NCH_2CH_2N). ^{13}C NMR (75 MHz, $CDCl_3$) *δ* 168.0, 164.3, 154.5, 150.3, 134.2, 132.2, 123.6, 108.6, 45.7, 44.1, 41.5 and 39.0. HR-MS (ESI) *m*/*z*: calcd for $C_{19}H_{18}N_4O_3$ $[M + H]^+$: 351.1457, found: 351.1343.

2-(2-(4-(4-Nitrophenyl)piperazin-1-yl)-2-oxoethyl)-isoindoline-1,3-dione PQM-190 (3h). Yellow solid (yield 28%), m.p. >300 °C. IR (ATR): *ν* 2973, 2956, 1775, 1712, 1651 and 1589 cm^{-1}. ^{1}H NMR (300 MHz, $CDCl_3$) *δ* 8.07 (d, *J* = 9.5 Hz, 2H, Ar–H), 7.85–7.93 (m, 4H, Ar–H), 7.02 (d, *J* = 9.5 Hz, 2H, Ar–H), 4.59 (s, 2H, CH_2CO), 3.75 (dd, *J* = 4.1 and 6.5 Hz, 2H NCH_2CH_2N), 3.60–3.57 (m, 4H, NCH_2CH_2N), 3.51 (dd, *J* = 3.8 and 7.5 Hz, 2H, NCH_2CH_2N), ^{13}C NMR (75 MHz, $CDCl_3$) *δ* 168.1, 165.0, 154.8, 137.5, 135.2, 132.1, 126.2, 123.8, 113.1, 46.4, 46.1 and 43.6. HR-MS (ESI) *m*/*z*: calcd for $C_{20}H_{18}N_4O_5$ $[M + Na]^+$: 417.1175, found: 417.1153.

In silico studies

Molecular docking study with AChE. We evaluated the possible binding modes of the compounds in the AChE binding site through molecular docking studies. Due to significant conformational changes observed on the peripheral anionic site (PAS),[60] we selected three representative conformations of AChE following an ensemble docking strategy adopted in a previous study[32,61] in addition to the structure of human AChE complexed with donepezil[62] (PDB code 4EY7). The ensemble docking strategy consists in docking the compounds into each representative conformation of the receptor, aiming to consider the protein flexibility.[63–65] The structures selected were 1ZGC[28] (*Torpedo californica*), 2CKM[29] (*Torpedo californica*), 1Q84 (ref. 30) (*Mus*

Table 4 Conserved waters considered in the docking experiments

Water	1ZGC	1Q84	2CKM	4EY7
Wat1	1468	1708	2062	729
Wat2	1481	1755	2054	737
Wat3	1489	1715	2061	722
Wat4	1531	1735	2035	731

musculus) and 4EY7 (ref. 62) (*Homo sapiens*). All inhibitors from the four representative conformations of AChE interact with both CAS and PAS. Conserved waters were identified through the superposition of the structures and considered explicitly during the docking experiments (Table 4).

The receptor structures were prepared using the protein preparation wizard tool from the Schrödinger suite 2018-4 (ref. 66) and the protonation states of the amino acid residues were predicted using PROPKA with pH 7. Finally, an optimization of the hydrogen bond network of the protein–ligand complexes was performed to adjust the orientation of the hydrogen atoms, followed by an energy minimization of the hydrogen atoms.

The compounds were designed and prepared using LigPrep from Maestro to set up the isomers, protonation states and tautomers with Epik[67,68] at pH 7.0 ± 0.4. We applied torsional constraints to some rotatable bonds to keep the planarity observed for some compounds during the docking experiments. The rotatable bond from the amide group was kept fixed to the *trans* conformation on all compounds.

The ensemble docking experiments were performed with the molecular docking program Glide[69] from Maestro in the XP precision mode, indicated for highly flexible ligands and to reduce false-positives. All the structures were aligned to the 1ZGC conformation using the super tool from Pymol. The receptor grids were centered on the native ligand present in the 1Q84 complex (*X*: 98.06, *Y*: 53.14 and *Z*: 22.06). We also redocked the co-crystallized ligands into their respective AChE conformation and to the non-native structures (*i.e.*, cross-docking) to validate the docking protocol, with all of them successfully predicted within 2.0 Å from the experimentally observed conformation. We selected the ligand pose according to the lowest XP score among all the four AChE conformations used for the ensemble docking protocol.

ADME prediction *in silico*. Based on 2D structural models drawn in ChemDraw professional version 15.0, ADME parameters were predicted *in silico* by using QikProp v. 3.5 (Schrödinger).

Biological evaluation

Anticholinesterase activity assays. Anticholinesterase activity was determined according to Ellman's method[27] modified for 96-well plates as previously described.[19] All solutions were prepared in Tris-HCl buffer (0.02 M, pH 7.5) and stock solutions of the test compounds were prepared in DMSO (50 mM). To 96-well plates were added solutions with the inhibitor compound at 30 μM final concentration. The vehicle control (DMSO final concentration 0.2% (v/v) for AChE) was used as reference (negative control) and the reagent 5,5′-dithiobis-2-nitrobenzoic acid (DTNB) was added to electric eel acetylcholinesterase (eeAChE) or equine serum butyrylcholinesterase (eqBuChE) in the presence of bovine serum albumin (BSA). Absorbance was recorded using an iMark plate reader (Bio-Rad) equipped with a light filter of 415 nm and this measurement was used as a blank reference. After 10 min of incubation at room temperature, acetylthiocholine iodide (ACTI) or *S*-butyrylthiocholine iodide (BCTI) was added and absorbance was recorded after 10 min of incubation at room temperature at λ = 415 nm 3 times within 30 s. Enzyme activity was calculated as a percentage of the mean absorbance values measured for the DMSO-treated control, discounted from the mean blank reference values. Assays were performed in triplicate (for standard deviation calculation). Inhibition values were calculated using the Excel program.

Kinetic assay. Enzyme kinetics was determined according to Ellman's method[27] modified for 96-well plates as previously described.[18,19] Both enzymes, acetylcholinesterase from *Electrophorus electricus* (electric eel) and butyrylcholinesterase from equine serum, were purchased from Sigma Aldrich. All solutions were prepared in Tris-HCl buffer (0.02 M, pH 7.5) and the stock solutions of the test compounds were prepared in DMSO (2 mM). To 96-well plates were added 150 μL inhibitor compound solution of compound **3g** at two different concentrations (2 and 4 μM) distributed in eight sets of triplicates each. Eight sets of DMSO-treated and untreated triplicates (final concentration 0.2% (v/v) AChE) were used as negative control. Subsequently, 60 μL of DTNB (Ellman's reagent) was added to 1.1 mM and 30 μL of isolate eeAChE at 0.20 U mL^{-1} in the presence of 1 mg mL^{-1} bovine serum albumin (BSA). Absorbance was then recorded using an iMark plate reader (Bio-Rad) equipped with a λ = 415 nm light filter and this measurement was used as a blank reference. After 10 min of incubation at 25 °C, 24 μL of acetylcholine iodide (ACTI) substrate at eight serially diluted concentrations (factor = 1.3) of 2.75–0 44 mM (final concentration: 0.25–0.04 mM) were added to the respective wells and the absorbance was recorded after incubation for 10 min at 25 °C at λ = 415 nm. Lineweaver–Burk reciprocal plots were obtained by plotting 1/velocity *versus* 1/[substrate] and two different inhibitor concentrations for the untreated control. The linear regression of each data set showed convergent behavior, whereby the region where the curves converge determines the type of inhibition. The values of K_i, K_i' (competitive and non-competitive inhibition constants, respectively), K_m (Michaelis–Menten constant) and V_{max} (maximum speed) were calculated with GraphPad Prism 7.0 using nonlinear regression models for kinetics, enzymatic inhibition and enzymatic kinetics, and substrate *versus* velocity.

DPPH scavenging activity. The ability of compounds PQM-183 to PQM-190 (**3a–h**) to scavenge DPPH free radicals was evaluated according to the method described by Gontijo 2012.[70] All compounds were evaluated at the concentrations of 200, 100, 50, 25, 12.5, 6.25, 3.13 and 1.56 μM in ethanol. A 4 mL aliquot of each sample was mixed with 1 mL of DPPH

(0.5 mM in ethanol). The solution was vigorously stirred at room temperature and after 30 min the absorbance was measured at 517 nm in a UV-vis spectrophotometer (Shimadzu). A low absorbance value indicates effective free radical scavenging. Each solution was analyzed in triplicate and the mean values were plotted to obtain the EC_{50} against DPPH by linear regression. Antioxidants like ascorbic acid and Trolox were used as a standard over the same range of concentrations. The radical-scavenging activity was evaluated as the percentage of inhibition according to the following equation: % inhibition = [(absorbance of control − absorbance of sample)/absorbance of control] × 100.

PAMPA assay

The model mimics the blood–brain barrier (PAMPA BBB). This assay is based on a two 96-well plate apparatus in a "sandwich"-type system, where one plate overlaps the other. The upper plate, called the donor compartment, refers to the place where the compounds (test or controls) are diluted in a buffered medium, which is characterized by the presence of a synthetic membrane of PVDF (polyvinylidene fluoride) impregnated with a lipid solution, forming a barrier through which the compounds migrate through a diffusion process to the bottom plate called the receptor.[37,71] The lipid mixture that impregnates the PVDF filter has a different constitution for the BBB (porcine polar membrane lipid extract in dodecane) and GIT (L-α soy phosphatidylcholine in dodecane) tests. In a 5 ml glass vial, 1 mg of each compound (test or control) was dissolved in 1 ml of ethanol. Then, 500 μL of ethanol and 3.5 mL of PBS pH 7.4 were added to this solution. The solutions were filtered (PVDF filter: 0.45 μM) and set aside. Subsequently, the acceptor 96-well microplate was filled with 180 μL of a solution of PBS pH 7.4 : ethanol (70 : 30). The donor 96-well plate was coated with 5 μL of porcine brain lipid in dodecane (20 mg lipid per mL, in dodecane). After 5 min, the donor plate received, in triplicate, 180 μL of the solution containing each compound. Then, the donor plate was carefully placed over the recipient, forming a sandwich-type system, which was left to rest for 2 h and 45 min at room temperature (±25 °C) and humidified. After incubation, the donor plate was removed and the concentration of all the compounds in both the acceptor and the donor wells was determined using the UV plate reader, which was read (SpectraMax 5® molecular devices) at the wavelengths previously established for each compound. The blank was prepared in the presence of 180 μL of PBS solution (pH 7.4) : ethanol (70 : 30) (adapted from Li Di's work[40]). The optical density values and data analysis were performed in the same manner as described previously in Lopes' work in 2019.[72]

Permeability studies were performed in the same manner as described previously in Lopes' work in 2019.[72] In the model mimicking intestinal permeability (PAMPA GIT), the lipid used was L-α soy phosphatidylcholine in dodecane. Then, in a 5 mL glass vial, 250 μL of the freshly prepared solution was homogenized with 4750 μL PBS (pH 6.6) at 10 μM. The solution was then filtered (PVDF filter: 0.45 μM) and reserved. Subsequently, 180 μL of a PBS (pH 7.4) : DMSO (95 : 5) solution was added to the wells of the recipient plate and 5 μL of soybean L-α-phosphatidylcholine lipid solution (20 mg lipid per mL in dodecane) to the wells of the donor plate. The filter plate was coupled to the receiver plate and was stirred at 50 rpm for 8 h at room temperature. Both experiments were performed in triplicate and two different analyses (n = 2) were performed in the presence of the control compounds.[73]

In vitro studies

Cell cultures. Monkey kidney epithelial VERO cells (CCL) were routinely grown in Dulbecco's modified Eagle's medium supplemented with 10% fetal bovine serum, 2 mM L-glutamine, 50 U mL^{-1} penicillin and 50 μg mL^{-1} streptomycin at 37 °C in a humidified incubator with 5% CO_2. Human neuronal (SH-SY5Y) cells were purchased from the Lombardy and Emilia Romagna Experimental Zootechnic Institute (Italy). SH-SY5Y cells were routinely grown in Dulbecco's modified Eagle's medium supplemented with 10% fetal bovine serum, 2 mM L-glutamine, 50 U mL^{-1} penicillin and 50 μg mL^{-1} streptomycin at 37 °C in a humidified incubator with 5% CO_2. SH-SY5Y cells were differentiated into neuron-like cells with retinoic acid (RA, 10 μM) for 6 days.[74]

Human monocyte THP-1 cells were purchased from Cell Bank Interlab Cell Line Collection (Italy). THP-1 cells were routinely grown in Roswell Park Memorial Institute (RPMI) 1640 medium with phenol red supplemented with 10% fetal bovine serum, 2 mM L-glutamine, 50 U mL^{-1} penicillin and 50 μg mL^{-1} streptomycin at 37 °C in a humidified incubator with 5% CO_2. THP-1 cells were differentiated into microglial-like cells with phorbol 12-myristate 13-acetate (PMA, 5 ng mL^{-1}) for 24 h at 37 °C in 5% CO_2.

Cytotoxicity assays. Cell viability, in terms of mitochondrial metabolic function, was evaluated by the reduction of 3-(4,5-dimethyl-2-thiazolyl)-2,5-diphenyl-2*H*-tetrazolium bromide (MTT) to its insoluble formazan, as previously described.[75] Briefly, neuronal SH-SY5Y cells were seeded in a 96-well plate at 2 × 10^4 cells per well, while epithelial VERO cells were seeded at 1 × 10^4 cells per well. Cell cultures were incubated for 24 h before the treatment with the test compounds. Subsequently, SH-SY5Y cells were treated for 24 h with different concentrations of compounds **3a–h** (2.5–80 μM), while VERO cells were treated for 48 h with different concentrations of the test compound **3g** (1.4–1428 μM) at 37 °C in 5% CO_2. Then the treatment medium was replaced with MTT solution (0.5 mg mL^{-1}) in Hank's Balanced Salt Solution (HBSS) for 2 h at 37 °C in 5% CO_2. After washing with HBSS, formazan crystals were dissolved in isopropanol. The amount of formazan was measured (570 nm, reference filter 690 nm) using a multilabel plate reader (VICTOR™ X3, PerkinElmer, Waltham, MA, USA) and an Anthos Zenyth 200rt microplate reader (Biochrom, UK). The cytotoxicity of the test compound was obtained using the following formula: $[(A - B)/A \times 100]$, where A represents the absorbance of untreated cells and B the absorbance of cells

treated with different concentrations of the test compounds. Cytotoxic concentration in 50% of cells was determined by linear regression.

Inflammation and neuronal plasticity assay. The anti-inflammatory activity of the test compound **3g** was evaluated in microglial THP-1 activated by LPS as previously described.[76] Briefly, THP-1 cells were seeded in a 6-well plate at 2.5×10^6 cells per well, incubated for 24 h with PMA (5 ng mL^{-1}) and subsequently treated for 24 h with LPS (1 μg mL^{-1}) in the presence of compound **3g** (10 μM). The neuronal plasticity of compound **3g** was evaluated in differentiated SH-SY5Y. Cells were seeded in 100 mm dishes at 1×10^6 cells per dish, differentiated with RA (10 μM) and subsequently treated for 24 h with compound **3g** (10 μM). Afterward, the cell suspension was pelleted, and RNA was extracted using a PureLink RNA Mini Kit (Life Technologies, Carlsbad, CA, USA) according to the manufacturer's guidelines. A total of 1 μg of RNA was used to synthesize cDNA using SuperScript VILO MasterMix (Invitrogen, Carlsbad, CA, USA). Quantitative RT-PCR was carried out using SYBR Select Master Mix (Invitrogen), and relative normalized expression was calculated by comparing the cycle threshold (C_t) of the target gene (inducible nitric oxide synthase (iNOS); Interleukin 1 beta (IL-1β); prostaglandin-endoperoxide synthase 2 (COX-2); synaptophysin (SYP); brain derived neurotrophic factor (BDNF)) to that of the reference genes β-actin and glyceraldehyde-3-phosphate dehydrogenase protein (GAPDH, Life Technologies). All reactions had three technical replicates, and each condition had three biological replicates. Relative quantification was calculated according to the $\Delta\Delta C_t$ method ($2^{-\Delta\Delta C_t}$) with untreated cells as control. Primer sequences used in this study are listed in Table 5.

***In vitro* activity against Aβ-aggregates.** In order to evaluate the activity of PQM-189 (**3g**) in the aggregation of $A\beta_{1-42}$ peptides, an *in vitro* assay was performed using the marker thioflavin T (ThT). It is a deep yellow pigment that is widely used to visualize and quantify the presence of misfolded protein aggregates (amyloid plaques) *in vivo* and *in vitro*. When connected to a structure rich in β-sheets, thioflavin exhibits an increase in fluorescence and a characteristic red shift of the emission spectrum in the 490 nm range when associated with aggregates (Wall *et al.*, 1999).[77] The fluorescence behavior of ThT may be caused by several factors, which can affect the state charge distribution of the compound when excited, including the association with rigid and highly ordered amyloid structures, or a specific chemical interaction with another protein (Khurana *et al.*, 2005).[78] This marker was diluted in a glycine–NaOH pH 8.5 solution for immediate reading, in the final concentration of 314 μM.

This protocol was adapted from Benseny Cases *et al.* (2012).[79] First, $A\beta_{1-42}$ peptide (BioNTech, Brazil) was dissolved in Milli-Q pH 10, divided into 75 μM aliquots, adjusted to pH 4–5 with HCl solution (2 μL), and stored at −80 °C until use.

Before the depolymerization assay, the $A\beta_{1-42}$ solution was incubated in a dry bath at 37 °C for 24 h. On the day of reading, a dark 96-well plate was used and 50 μL $A\beta_{1-42}$ solution (75 μM) was added as well as 50 μL ThT, 50 μL of PQM-189 (**3g**) and water to make up to 300 μL. The compound was tested in 3 doses (75 μM). Using a FlexStation reader (American Molecular Equipment Company), single-point reading and polymerization analysis were performed at 37 °C with 450 nm excitation wavelength and 490 nm emission wavelength, and then kinetic readings were conducted for 1 h. The readings were performed every 15 min under the previously described conditions; the interaction was observed every 15 min for 1 h. The whole process was carried out in a dark environment so as not to interfere with ThT fluorescence. All experiments were carried out in experimental triplicates as well as in three independent experiments. The results were analyzed using GraphPad Prism® 9.0 software (San Diego, CA, USA). The results obtained when reading the endpoint in the FlexStation were subjected to one-way analysis of variance (ANOVA) followed by the Tukey test. The evaluation of data at different times was performed by using two-way ANOVA followed by the Bonferroni test. For all data, values where $p < 0.05$ were considered significant.

Table 5 Primer sequences for quantitative RT-PCR

Gene name	Forward/reverse	5′ to 3′ sequence
iNOS	For	TGAACTACGTCCTGTCCCCT
	Rev	CTCTTCTCTTGGGTCTCCGC
IL-1β	For	TGATGGCTTATTACAGTGGCAATG
	Rev	GTAGTGGTGGTCGGAGATTGC
COX-2	For	CAAATCCTTGCTGTTCCCACCCAT
	Rev	GTGCACTGTGTTTGGAGTGGGTTT
SYP	For	GCAGCGGTGGCAGTGGC
	Rev	GGACGGGGTAAGAGAGGGG
BDNF	For	CAAAAGTGGAGAACATTTGC
	Rev	AACTCCAGTCAATAGGTCAG
B-Actin	For	GCGAGAAGATGACCCAGATC
	Rev	GGATAGCACAGCCTGGATAG
GAPDH	For	GGTCGGAGTCAACGGATTTG
	Rev	GGAAGATGGTGATGGGATTTC

***In vivo* studies: animals.** Adult male Wistar rats ($n = 7$ per group) were obtained from the Central Animal Facility of the Federal University of Alfenas and housed under controlled light (12 : 12 h light–dark cycle; lights on at 7:00 a.m.) and temperature conditions (23 ± 2 °C) with access to water and food except for the night before the experiments when they were submitted to an overnight fast (8 h). The experiments were performed according to the Brazilian Guidelines for Animal Experimentation defined by the National Council for Animal Experimentation Control. The experimental protocol was approved by the local Research Ethics Committee of the Federal University of Alfenas (protocol 15/2019).

Experimental design. On the day of the test, the feed was removed, and the adult male Wistar rats received vehicle or **3g** by gavage and then LPS or saline by intraperitoneal administration. After 2 h, they were submitted to the open field and the previously weighed pelleted feed was reintroduced. The pattern of food intake was monitored and after 24 h the adult male rats were euthanized to collect brain structures.

Feeding behavior. Before the test day, the adult male Wistar rats were placed in individual boxes and had free access to water and food. On the day of the test, before receiving treatment, the food was removed for 2 h. After this feeding restriction, the animals were offered pre-weighed pelleted feed and the pattern of food intake was monitored for 24 h by weighing the feed at 2, 4, 6 and 24 h after its reintroduction.[80]

Open field behavioral test. The aim of this test could verify the locomotor activity in rats to discard the possible nonspecific muscle relaxant or sedative effects. Groups of rats (n = 8) were treated with vehicle 1 h before the test. Each rat (n = 8 per group) was placed in the center of a circular black-bottomed apparatus (60 cm in diameter and 60 cm high walls) and filmed with a digital video camera for 5 min. The analysis was performed using Ethovision XT 9.0 software (computerized observation system capable of measuring locomotor behavior), where we analyzed the distance traveled by the adult male Wistar rats in the arena and their immobility time.[81]

Statistical analysis. Data were analyzed using the software program GraphPad version 9.0 and expressed as mean ± standard error of the mean (SEM). To compare the effect of LPS and pretreatment with compound **3g** *in vivo*, two-way ANOVA was used followed by the Bonferroni post-test. In the *in vitro* study, one-way ANOVA was used followed by the Bonferroni post-test. The level of significance was based on p values less than 0.05 ($p < 0.05$).

Conclusions

Currently, it is very well documented that neuroinflammation plays a central role in both early and late stages of AD-related neurodegeneration. In this sense, an anti-inflammatory pharmacological approach, coupled to neuroprotection and AChE inhibition could be of clinical relevance in a disease-modifying intervention aiming to effectively control the progression of AD. We reported the discovery of PQM-189 (**3g**), designed as a new multifunctional thalidomide–donepezil hybrid compound, with a unique structural architecture and significant neuroprotective and selective AChE inhibitory properties, aside from anti-neuroinflammatory effects evidenced in different *in vitro* and *in vivo* models. In addition, compound **3g** did not exhibit any significant cytotoxicity in different assays. Besides the ability of inhibiting AChE in a selective and mixed mode, compound **3g** exhibited the ability to inhibit iNOS and IL-1β, two important mediators of AD-related brain inflammation. According to the multiple factors related to the pathogenesis of NDs, compound PQM-189 (**3g**) could represent a promising drug prototype candidate. This compound is suggested for further studies in drug discovery and development of genuine multi-target-directed drugs for ND therapeutics.

Conflicts of interest

The authors declare that there are no conflicts of interest.

Acknowledgements

The authors are grateful to the Brazilian Agencies CNPq (#454088/2014-0, #400271/2014-1, #310082/2016-1, #406739/2018-8 and #303804/2020-3), FAPEMIG (#CEX-APQ-00241-15 and #CEX - APQ-00518-17), FINEP, INCT-INOFAR (#465.249/2014-0), and PRPPG-UNIFAL for financial support and fellowships. This study was also financed in part by the Coordenação de Aperfeiçoamento de Pessoal de Nível Superior – Brazil (CAPES) – Finance Code 001.

References

1 R. Businaro, M. Corsi, R. Asprino, C. Di Lorenzo, D. Laskin, R. M. Corbo, S. Ricci and A. Pinto, Modulation of Inflammation as a Way of Delaying Alzheimer's Disease Progression: The Diet's Role, *Curr. Alzheimer Res.*, 2018, **15**(4), 363–380.

2 G. Gelders, V. Baekelandt and A. Van der Perren, Linking Neuroinflammation and Neurodegeneration in Parkinson's Disease, *J. Immunol. Res.*, 2018, **2018**, 1–12.

3 C. Lois, I. González, D. Izquierdo-García, N. R. Zürcher, P. Wilkens, M. L. Loggia, J. M. Hooker and H. D. Rosas, Neuroinflammation in Huntington's Disease: New Insights with 11C-PBR28 PET/MRI, *ACS Chem. Neurosci.*, 2018, **9**(11), 2563–2571.

4 S. Haase and R. A. Linker, Inflammation in Multiple Sclerosis, *Ther. Adv. Neurol. Disord.*, 2021, **14**, 1–16.

5 D. Yates, Neurodegenerative Disease: A Proteostatic Boost, *Nat. Rev. Neurosci.*, 2018, **19**(2), 61.

6 R. Fischer and O. Maier, Interrelation of Oxidative Stress and Inflammation in Neurodegenerative Disease: Role of TNF, *Oxid. Med. Cell. Longevity*, 2015, **2015**, 1–18.

7 M. Schain and W. C. Kreisl, Neuroinflammation in Neurodegenerative Disorders—a Review, *Curr. Neurol. Neurosci. Rep.*, 2017, **17**(3), 25.

8 Z. Liu, T. Zhou, A. C. Ziegler, P. Dimitrion and L. Zuo, Oxidative Stress in Neurodegenerative Diseases: From Molecular Mechanisms to Clinical Applications, *Oxid. Med. Cell. Longevity*, 2017, **2017**, 1–11.

9 J. N. Cobley, M. L. Fiorello and D. M. Bailey, 13 Reasons Why the Brain Is Susceptible to Oxidative Stress, *Redox Biol.*, 2018, **15**, 490–503.

10 R. Minhas, Y. Bansal and G. Bansal, Inducible Nitric Oxide Synthase Inhibitors: A Comprehensive Update, *Med. Res. Rev.*, 2020, **40**(3), 823–855.

11 T. Nakamura and S. A. Lipton, Protein S-Nitrosylation as a Therapeutic Target for Neurodegenerative Diseases, *Trends Pharmacol. Sci.*, 2016, **37**(1), 73–84.

12 I. Soufli, R. Toumi, H. Rafa and C. Touil-Boukoffa, Overview of Cytokines and Nitric Oxide Involvement in Immuno-Pathogenesis of Inflammatory Bowel Diseases, *World J. Gastrointest. Pharmacol. Ther.*, 2016, **7**(3), 353.

13 M. E. Kim, J. Y. Na, Y. D. Park and J. S. Lee, Anti-Neuroinflammatory Effects of Vanillin Through the Regulation of Inflammatory Factors and NF-KB Signaling in

LPS-Stimulated Microglia, *Appl. Biochem. Biotechnol.*, 2019, **187**(3), 884–893.
14 M. Reale and E. Costantini, Cholinergic Modulation of the Immune System in Neuroinflammatory Diseases, *Diseases*, 2021, **9**(2), 29.
15 R. Benfante, S. Di Lascio, S. Cardani and D. Fornasari, Acetylcholinesterase Inhibitors Targeting the Cholinergic Anti-Inflammatory Pathway: A New Therapeutic Perspective in Aging-Related Disorders, *Aging: Clin. Exp. Res.*, 2021, **33**(4), 823–834.
16 M. de Freitas Silva, K. S. T. Dias, V. S. Gontijo, C. J. C. Ortiz and C. Viegas, Multi-Target Directed Drugs as a Modern Approach for Drug Design Towards Alzheimer's Disease: An Update, *Curr. Med. Chem.*, 2018, **25**(29), 3491–3525.
17 N. Vargesson, Thalidomide-induced Teratogenesis: History and Mechanisms, *Birth Defects Res., Part C*, 2015, **105**(2), 140–156.
18 G. A. de Souza, S. J. da Silva, C. N. de Del Cistia, P. Pitasse-Santos, L. O. de Pires, Y. M. Passos, Y. Cordeiro, C. M. Cardoso, R. N. Castro, C. M. R. Sant'Anna and A. E. Kümmerle, Discovery of Novel Dual-Active 3-(4-(Dimethylamino)Phenyl)-7-Aminoalcoxy-Coumarin as Potent and Selective Acetylcholinesterase Inhibitor and Antioxidant, *J. Enzyme Inhib. Med. Chem.*, 2019, **34**(1), 631–637.
19 S. N. Santos, G. Alves de Souza, T. M. Pereira, D. P. Franco, C. de Nigris Del Cistia, C. M. R. Sant'Anna, R. B. Lacerda and A. E. Kümmerle, Regioselective Microwave Synthesis and Derivatization of 1,5-Diaryl-3-Amino-1,2,4-Triazoles and a Study of Their Cholinesterase Inhibition Properties, *RSC Adv.*, 2019, **9**(35), 20356–20369.
20 L. Kabasakal and S. Alan, Thalidomide Attenuates Learning and Memory Defi Cits Induced by Intracerebroventricular Administration of Streptozotocin in Rats, *Biotech. Histochem.*, 2012, **88**(3–4), 145–152.
21 G. Palencia, J. Ángel, N. Medrano, A. Ortiz-plata, D. Jiménez, J. Sotelo, A. Sánchez and C. Trejo-solís, Anti-Apoptotic, Anti-Oxidant, and Anti-Inflammatory Effects of Thalidomide on Cerebral Ischemia/Reperfusion Injury in Rats, *J. Neurol. Sci.*, 2015, **351**(1–2), 78–87.
22 F. A. Luzzio, Thalidomide and Analogues, in *Imides Medicinal, Agricultural, Synthetic Applications and Natural Products Chemistry*, ed. F. A. Luzzio and M. B. Smith, Elsevier, Amsterdam, The Netherlands, 1st edn, 2019, vol. 1, pp. 404–405.
23 J. J. Casal, M. Bollini, M. E. Lombardo and A. M. Bruno, Thalidomide Analogues: Tumor Necrosis Factor-Alpha Inhibitors and Their Evaluation as Anti-Inflammatory Agents, *Eur. J. Pharm. Sci.*, 2016, **83**, 114–119.
24 V. C. Silva and A. Giusti-Paiva, Sickness Behavior Is Delayed in Hypothyroid Mice, *Brain, Behav., Immun.*, 2015, **45**, 109–117.
25 T. Q. Pham, P. Berghofer, X. Liu, I. Greguric, B. Dikic, P. Ballantyne, F. Mattner, V. Nguyen, C. Loc'h and A. Katsifis, Preparation and Biologic Evaluation of a Novel Radioiodinated Benzylpiperazine, 123I-MEL037, for Malignant Melanoma, *J. Nucl. Med.*, 2007, **48**(8), 1348–1356.
26 K. Kamiński, J. Obniska, B. Wiklik and D. Atamanyuk, Synthesis and Anticonvulsant Properties of New Acetamide Derivatives of Phthalimide, and Its Saturated Cyclohexane and Norbornene Analogs, *Eur. J. Med. Chem.*, 2011, **46**(9), 4634–4641.
27 G. L. Ellman, K. D. Courtney, V. Andres and R. M. Featherstone, A New and Rapid Colorimetric Determination of Acetylcholinesterase Activity, *Biochem. Pharmacol.*, 1961, **7**(2), 88–95.
28 H. Haviv, D. M. Wong, H. M. Greenblatt, P. R. Carlier, Y. P. Pang, I. Silman and J. L. Sussman, Crystal Packing Mediates Enantioselective Ligand Recognition at the Peripheral Site of Acetylcholinesterase, *J. Am. Chem. Soc.*, 2005, **127**(31), 11029–11036.
29 E. H. Rydberg, B. Brumshtein, H. M. Greenblatt, D. M. Wong, D. Shaya, L. D. Williams, P. R. Carlier, Y. P. Pang, I. Silman and J. L. Sussman, Complexes of Alkylene-Linked Tacrine Dimers with Torpedo Californica Acetylcholinesterase: Binding of Bis(5)-Tacrine Produces a Dramatic Rearrangement in the Active-Site Gorge, *J. Med. Chem.*, 2006, **49**(18), 5491–5500.
30 Y. Bourne, H. C. Kolb, Z. Radić, K. B. Sharpless, P. Taylor and P. Marchot, Freeze-Frame Inhibitor Captures Acetylcholinesterase in a Unique Conformation, *Proc. Natl. Acad. Sci. U. S. A.*, 2004, **101**(6), 1449–1454.
31 M. Harel, I. Schalk, L. Ehret-Sabatier, F. Bouet, M. Goeldner, C. Hirth, P. H. Axelsen, I. Silman and J. L. Sussman, Quaternary Ligand Binding to Aromatic Residues in the Active-Site Gorge of Acetylcholinesterase, *Proc. Natl. Acad. Sci. U. S. A.*, 1993, **90**(19), 9031–9035.
32 M. A. Ceschi, J. S. da Costa, J. P. B. Lopes, V. S. Câmara, L. F. Campo, A. C. A. de Borges, C. A. S. Gonçalves, D. F. de Souza, E. L. Konrath, A. L. M. Karl, I. A. Guedes and L. E. Dardenne, Novel Series of Tacrine-Tianeptine Hybrids: Synthesis, Cholinesterase Inhibitory Activity, S100B Secretion and a Molecular Modeling Approach, *Eur. J. Med. Chem.*, 2016, **121**, 758–772.
33 Z. Liu, L. Fang, H. Zhang, S. Gou and L. Chen, Design, Synthesis and Biological Evaluation of Multifunctional Tacrine-Curcumin Hybrids as New Cholinesterase Inhibitors with Metal Ions-Chelating and Neuroprotective Property, *Bioorg. Med. Chem.*, 2017, **25**(8), 2387–2398.
34 J. Kujawski, H. Popielarska, A. Myka, B. Drabińska and M. Bernard, The Log P Parameter as a Molecular Descriptor in the Computer-Aided Drug Design – an Overview, *Computational Methods in Science and Technology*, 2012, **18**(2), 81–88.
35 S. Rourou, M. Ben Zakkour and H. Kallel, Adaptation of Vero Cells to Suspension Growth for Rabies Virus Production in Different Serum Free Media, *Vaccine*, 2019, **37**(47), 6987–6995.
36 N. C. Ammerman, M. Beier-Sexton and A. F. Azad, Growth and Maintenance of Vero Cell Lines, *Curr. Protoc. Microbiol.*, 2008, **11**, A.4E.1–A.4E.7.
37 A. Fortuna, G. Alves, P. Soares-da-silva and A. Falcão, Optimization of a Parallel Artificial Membrane Permeability Assay for the Fast and Simultaneous Prediction of Human Intestinal Absorption and Plasma Protein Binding of Drug Candidates: Application to Dibenz[b,f]Azepine-5-Carboxamide Derivatives, *J. Pharm. Sci.*, 2012, **101**(2), 530–540.

38 D. I. Pérez, M. Pistolozzi, V. Palomo, M. Redondo, C. Fortugno, C. Gil, G. Felix, A. Martinez and C. Bertucci, 5-Imino-1,2-4-Thiadiazoles and Quinazolines Derivatives as Glycogen Synthase Kinase 3β(GSK-3β) and Phosphodiesterase 7(PDE7) Inhibitors: Determination of Blood-Brain Barrier Penetration and Binding to Human Serum Albumin, *Eur. J. Pharm. Sci.*, 2012, **45**(5), 677–684.

39 M. Kansy, F. Senner and K. Gubernator, Physicochemical High Throughput Screening: Parallel Artificial Membrane Permeation Assay in the Description of Passive Absorption Processes, *J. Med. Chem.*, 1998, **41**(7), 1007–1010.

40 L. Di, E. H. Kerns, K. Fan, O. J. McConnell and G. T. Carter, High Throughput Artificial Membrane Permeability Assay for Blood-Brain Barrier, *Eur. J. Med. Chem.*, 2003, **38**(3), 223–232.

41 K. R. Doty, M.-V. Guillot-Sestier and T. Town, The Role of the Immune System in Neurodegenerative Disorders: Adaptive or Maladaptive?, *Brain Res.*, 2015, **1617**, 155–173.

42 E. Kozela, A. Juknat and Z. Vogel, Modulation of Astrocyte Activity by Cannabidiol, a Nonpsychoactive Cannabinoid, *Int. J. Mol. Sci.*, 2017, **18**(8), 1669.

43 H. Akiyama, S. Barger and S. Barnum, *et al.*, Inflammation and Alzheimer's Disease, *Neurobiol. Aging*, 2000, **21**(3), 383–421.

44 M. Bolós, J. R. Perea and J. Avila, Alzheimer's Disease as an Inflammatory Disease, *Biomol. Concepts*, 2017, **8**(1), 37–43.

45 S. Shi, Z. Wang and Z. Qiao, The Multifunctional Anti-Inflammatory Drugs Used in the Therapy of Alzheimer's Disease, *Curr. Med. Chem.*, 2013, **20**(20), 2583–2588.

46 C. K. Glass, K. Saijo, B. Winner, M. C. Marchetto and F. H. Gage, Mechanisms Underlying Inflammation in Neurodegeneration, *Cell*, 2010, **140**(6), 918–934.

47 J. Zhang and S. Rivest, Is Survival Possible Without Arachidonate Metabolites in the Brain During Systemic Infection?, *Physiology*, 2003, **18**(4), 137–142.

48 T. Oka, K. Oka, T. E. Scammell, C. Lee, J. F. Kelly, F. Nantel, J. K. Elmquist and C. B. Saper, Relationship of EP1-4 Prostaglandin Receptors with Rat Hypothalamic Cell Groups Involved in Lipopolysaccharide Fever Responses, *J. Comp. Neurol.*, 2000, **428**(1), 20–32.

49 S. Rivest, How Circulating Cytokines Trigger the Neural Circuits That Control the Hypothalamic-Pituitary-Adrenal Axis, *Psychoneuroendocrinology*, 2001, **26**(8), 761–788.

50 R. Dantzer, Cytokine, Sickness Behavior, and Depression, *Immunol. Allergy Clin. North Am.*, 2009, **29**(2), 247–264.

51 D. M. Norden, P. J. Trojanowski, E. Villanueva, E. Navarro and J. P. Godbout, Sequential Activation of Microglia and Astrocyte Cytokine Expression Precedes Increased Iba-1 or GFAP Immunoreactivity Following Systemic Immune Challenge, *Glia*, 2016, **64**(2), 300–316.

52 B. L. Hart, Biological Basis of the Behavior of Sick Animals, *Neurosci. Biobehav. Rev.*, 1988, **12**(2), 123–137.

53 S. Kent, R. M. Bluthé, K. W. Kelley and R. Dantzer, Sickness Behavior as a New Target for Drug Development, *Trends Pharmacol. Sci.*, 1992, **13**(C), 24–28.

54 R. Schliebs and T. Arendt, The Cholinergic System in Aging and Neuronal Degeneration, *Behav. Brain Res.*, 2011, **221**(2), 555–563.

55 M. T. Golia, S. Poggini, S. Alboni, S. Garofalo, N. Ciano Albanese, A. Viglione, M. A. Ajmone-Cat, A. St-Pierre, N. Brunello, C. Limatola, I. Branchi and L. Maggi, Interplay between Inflammation and Neural Plasticity: Both Immune Activation and Suppression Impair LTP and BDNF Expression, *Brain, Behav., Immun.*, 2019, **81**, 484–494.

56 O. Sheppard, M. P. Coleman and C. S. Durrant, Lipopolysaccharide-Induced Neuroinflammation Induces Presynaptic Disruption through a Direct Action on Brain Tissue Involving Microglia-Derived Interleukin 1 Beta, *J. Neuroinflammation*, 2019, **16**(1), 1–13.

57 F. Wang, Z. Wu, X. Zha, Y. Cai, B. Wu, X. Jia and D. Zhu, Concurrent Administration of Thyroxine and Donepezil Induces Plastic Changes in the Prefrontal Cortex of Adult Hypothyroid Rats, *Mol. Med. Rep.*, 2017, **16**(3), 3233–3241.

58 F. Vasilopoulou, S. Rodríguez-Arévalo, A. Bagán, C. Escolano, C. Griñán-Ferré and M. Pallàs, Disease-Modifying Treatment with I2 Imidazoline Receptor Ligand LSL60101 in an Alzheimer's Disease Mouse Model: A Comparative Study with Donepezil, *Br. J. Pharmacol.*, 2021, **178**(15), 3017–3033.

59 A. K. Singh, B. Rathi, V. V. Medviediev, O. V. Shishkin, V. Bahadur, T. Singh, B. K. Singh, N. Vijayan, V. Balachandran and N. Y. Gorobets, Functionalized Organic Frameworks Explored as Second Order NLO Agents, *J. Chem. Sci.*, 2016, **128**(2), 297–309.

60 G. Johnson and S. Moore, The Peripheral Anionic Site of Acetylcholinesterase: Structure, Functions and Potential Role in Rational Drug Design, *Curr. Pharm. Des.*, 2006, **12**(2), 217–225.

61 J. P. B. Lopes, J. S. Da Costa, M. A. Ceschi, C. A. S. Gonçalves, E. L. Konrath, L. M. Karl, I. A. Guedes and L. E. Dardenne, Chiral Bistacrine Analogues: Synthesis, Cholinesterase Inhibitory Activity and a Molecular Modeling Approach, *J. Braz. Chem. Soc.*, 2017, **28**(11), 2218–2228.

62 J. Cheung, M. J. Rudolph, F. Burshteyn, M. S. Cassidy, E. N. Gary, J. Love, M. C. Franklin and J. J. Height, Structures of Human Acetylcholinesterase in Complex with Pharmacologically Important Ligands, *J. Med. Chem.*, 2012, **55**(22), 10282–10286.

63 I. A. Guedes, C. S. de Magalhães and L. E. Dardenne, Receptor-Ligand Molecular Docking, *Biophys. Rev.*, 2014, **6**(1), 75–87.

64 I. A. Guedes, F. S. S. Pereira and L. E. Dardenne, Empirical Scoring Functions for Structure-Based Virtual Screening: Applications, Critical Aspects, and Challenges, *Front. Pharmacol.*, 2018, **9**(SEP), 1–18.

65 I. R. Craig, J. W. Essex and K. Spiegel, Ensemble Docking into Multiple Crystallographically Derived Protein Structures: An Evaluation Based on the Statistical Analysis of Enrichments, *J. Chem. Inf. Model.*, 2010, **50**(4), 511–524.

66 G. Madhavi Sastry, M. Adzhigirey, T. Day, R. Annabhimoju and W. Sherman, Protein and Ligand Preparation: Parameters, Protocols, and Influence on Virtual Screening Enrichments, *J. Comput.-Aided Mol. Des.*, 2013, **27**(3), 221–234.

67 J. R. Greenwood, D. Calkins, A. P. Sullivan and J. C. Shelley, Towards the Comprehensive, Rapid, and Accurate Prediction

of the Favorable Tautomeric States of Drug-like Molecules in Aqueous Solution, *J. Comput.-Aided Mol. Des.*, 2010, **24**(6–7), 591–604.

68 J. C. Shelley, A. Cholleti, L. L. Frye, J. R. Greenwood, M. R. Timlin and M. Uchimaya, Epik: A Software Program for PK a Prediction and Protonation State Generation for Drug-like Molecules, *J. Comput.-Aided Mol. Des.*, 2007, **21**(12), 681–691.

69 R. A. Friesner, R. B. Murphy, M. P. Repasky, L. L. Frye, J. R. Greenwood, T. A. Halgren, P. C. Sanschagrin and D. T. Mainz, Extra Precision Glide: Docking and Scoring Incorporating a Model of Hydrophobic Enclosure for Protein –Ligand Complexes, *J. Med. Chem.*, 2006, **49**(21), 6177–6196.

70 V. S. Gontijo, T. C. De Souza, I. A. Rosa, M. G. Soares, M. A. Da Silva, W. Vilegas, C. Viegas and M. H. Dos Santos, Isolation and Evaluation of the Antioxidant Activity of Phenolic Constituents of the Garcinia Brasiliensis Epicarp, *Food Chem.*, 2012, **132**(3), 1230–1235.

71 X. Chen, A. Murawski, K. Patel, C. L. Crespi and P. V. Balimane, A Novel Design of Artificial Membrane for Improving the PAMPA Model, *Pharm. Res.*, 2008, **25**(7), 1511–1520.

72 J. P. B. Lopes, L. Silva, M. A. Ceschi, D. S. Lüdtke, A. R. Zimmer, T. C. Ruaro, R. F. Dantas, C. M. C. de Salles, F. P. Silva-Jr, M. R. Senger, G. Barbosa, L. M. Lima, I. A. Guedes and L. E. Dardenne, Synthesis of New Lophine–Carbohydrate Hybrids as Cholinesterase Inhibitors: Cytotoxicity Evaluation and Molecular Modeling, *MedChemComm*, 2019, **10**(12), 2089–2101.

73 C. Zhu, L. Jiang, T. M. Chen and K. K. Hwang, A Comparative Study of Artificial Membrane Permeability Assay for High Throughput Profiling of Drug Absorption Potential, *Eur. J. Med. Chem.*, 2002, **37**(5), 399–407.

74 A. Jämsä, K. Hasslund, R. F. Cowburn, A. Bäckström and M. Vasänge, The Retinoic Acid and Brain-Derived Neurotrophic Factor Differentiated SH-SY5Y Cell Line as a Model for Alzheimer's Disease-like Tau Phosphorylation, *Biochem. Biophys. Res. Commun.*, 2004, **319**(3), 993–1000.

75 L. Pruccoli, F. Morroni, G. Sita, P. Hrelia and A. Tarozzi, Esculetin as a Bifunctional Antioxidant Prevents and Counteracts the Oxidative Stress and Neuronal Death Induced by Amyloid Protein in Sh-Sy5y Cells, *Antioxidants*, 2020, **9**(6), 1–16.

76 R. M. C. Di Martino, L. Pruccoli, A. Bisi, S. Gobbi, A. Rampa, A. Martinez, C. Pérez, L. Martinez-Gonzalez, M. Paglione, E. Di Schiavi, F. Seghetti, A. Tarozzi and F. Belluti, Novel Curcumin-Diethyl Fumarate Hybrid as a Dualistic GSK-3β Inhibitor/Nrf2 Inducer for the Treatment of Parkinson's Disease, *ACS Chem. Neurosci.*, 2020, **11**(17), 2728–2740.

77 J. Wall, C. L. Murphy and A. Solomon, *In Vitro* Immunoglobulin Light Chain Fibrillogenesis, *Methods Enzymol.*, 1999, **309**, 204–217.

78 R. Khurana, C. Coleman, C. Ionescu-Zanetti, S. A. Carter, V. Krishna, R. K. Grover, R. Roy and S. Singh, Mechanism of Thioflavin T Binding to Amyloid Fibrils, *J. Struct. Biol.*, 2005, **151**(3), 229–238.

79 N. Benseny-Cases, O. Klementieva and J. Cladera, In Vitro Oligomerization and Fibrillogenesis of Amyloid-Beta Peptides, *Subcell. Biochem.*, 2012, **65**, 53–74.

80 R. Rorato, A. M. Menezes, A. Giusti-Paiva, M. De Castro, J. Antunes-Rodrigues and L. L. K. Elias, Prostaglandin Mediates Endotoxaemia-Induced Hypophagia by Activation of pro-Opiomelanocortin and Corticotrophin-Releasing Factor Neurons in Rats, *Exp. Physiol.*, 2009, **94**(3), 371–379.

81 L. P. J. J. Noldus, A. J. Spink and R. A. J. Tegelenbosch, EthoVision: A Versatile Video Tracking System for Automation of Behavioral Experiments, *Behav. Res. Methods Instrum. Comput.*, 2001, **33**(3), 398–414.

